Modeling climate-vegetation interactions during the last interglacial

Li, Huan; Renssen, Hans; Roche, Didier M.

published in
Quaternary Science Reviews
2020

DOI (link to publisher)
10.1016/j.quascirev.2020.106609

document version
Publisher's PDF, also known as Version of record

Quaternary Science Reviews 249 (2020) 106609

Contents lists available at ScienceDirect

Quaternary Science Reviews

journal homepage: www.elsevier.com/locate/quascirev

Modeling climate-vegetation interactions during the last interglacial: The impact of biogeophysical feedbacks in North Africa

Huan Li [a, b, *], Hans Renssen [b, c], Didier M. Roche [b, d]

[a] School of Geographic Science, Nantong University, Tongjingdadao 999, Nantong, 226007, China
[b] Vrije Universiteit Amsterdam, Faculty of Science, Cluster Earth and Climate, de Boelelaan 1085, Amsterdam, the Netherlands
[c] Department of Natural Sciences and Environmental Health, University of South-Eastern Norway, Gullbringvegen 36, N-3800, Bøi Telemark, Norway
[d] Laboratoire des Sciences du Climat et de l'Environnement, LSCE/IPSL, CEA-INSU-UVSQ-CNRS, Université Paris-Saclay, Gif-sur-Yvette, France

ARTICLE INFO

Article history:
Received 2 April 2020
Received in revised form
14 September 2020
Accepted 18 September 2020
Available online 28 September 2020

Keywords:
The last interglacial
Vegetation feedbacks
Regional and global scales
Simulations
North Africa

ABSTRACT

Previous climate model simulations of the early Last Interglacial (LIG) underestimated the temperatures compared to proxy-based reconstructions. One possible reason for this underestimation is that in these simulations the vegetation was prescribed to a pre-industrial state. To study the impact of climate-vegetation interactions, we performed a series of model experiments using the iLOVECLIM climate model, in which either VECODE or LPJ-GUESS was coupled as vegetation component. We specifically assessed the evolution of vegetation during the LIG and the magnitude of dynamical vegetation feedbacks. Our results show a relatively high vegetation cover (>70%) in the Sahara during the early LIG when the summer insolation at 20°N was high. This early stage is followed by an accelerated desertification phase after 123 ka BP. The rates of desertification in the Sahara peak at 122 ka BP, responding to the fast decline in 20°N July insolation. This desertification is accelerated when the magnitude of positive vegetation feedbacks on precipitation cannot offset the moisture deficit due to decreased summer insolation.

Simulations including the LIG vegetation feedback suggest warmer conditions than simulations with prescribed pre-industrial vegetation, but they still slightly underestimate the temperature suggested by proxy records. This is particularly the case in the high latitude regions and the tropics, where the 125 ka BP vegetation cover is significantly higher than the pre-industrial state. The magnitude of vegetation feedbacks in North Africa to local climate peaks in the early LIG and decreases during the LIG, corresponding to temporal vegetation changes. During the early LIG, experiments with dynamical vegetation suggested a doubling in the amount of precipitation (~60 cm/yr) in comparison to experiments with fixed pre-industrial vegetation. In addition, adding dynamical vegetation causes higher surface temperatures by about 2.5 °C in North Africa. At a global scale, a vegetated Sahara during the early LIG leads to an increase in surface temperature and a decline in surface air pressure due to local feedbacks, thereby enhancing mid-latitude westerlies as a result of increased latitudinal temperature and pressure gradient, leading to an increase in the amount of heat transported by the atmosphere from tropical regions to the Arctic. This green Sahara feedback provides 30% of the total contribution of global vegetation feedbacks to high latitudes warming.

1. Introduction

The last interglacial (LIG, ~130–116 ka BP) is characterized by about 2 °C higher global mean temperature (Turney and Jones, 2010) and higher sea level relative to pre-industrial conditions. At about 124 ka BP, this higher sea level reached a maximum of +6.6 m with 95% probability and +8.0 m with 67% probability (Kopp et al., 2009). The magnitude of this LIG climate warming and high sea level condition is comparable to the range of predicted future climates (Otto-Bliesner et al., 2017). Compared to the current interglacial (the Holocene), the LIG experienced stronger insolation changes (Berger, 1978), but had similar greenhouse gas (GHG) concentrations and continental configurations. These stronger

* Corresponding author. School of Geographic Science, Nantong University, Tongjingdadao 999, Nantong, 226007, China
E-mail address: huan.li.lzu@gmail.com (H. Li).

https://doi.org/10.1016/j.quascirev.2020.106609
0277-3791/

insolation changes resulted in a stronger seasonal contrast in the Northern Hemisphere (NH), giving rise to warmer summers and a significant enhancement of the NH monsoons during the LIG (Hely et al., 2014; Lezine et al., 2011; Saraswat et al., 2013; Tierney et al., 2017). Knowledge of the LIG climate thus provides valuable insights on the responses of the climate system under relatively "warm" forcing conditions. The LIG climate is therefore of interest to the Paleoclimate Modeling Intercomparison Project (PMIP, Otto-Bliesner et al., 2017) and has been studied extensively in both reconstructions (Andersen et al., 2004; CAPE Last Interglacial Project Members, 2006; Turney and Jones, 2010; McKay et al., 2011) and simulations (Schurgers et al., 2006, 2007; Gröger et al., 2007; Fischer and Jungclaus, 2010; Govin et al., 2012; Lunt et al., 2013; Nikolova et al., 2013; Otto-Bliesner et al., 2013; Bakker et al., 2013, 2014; Langebroek and Nisancioglu, 2014; Pedersen et al., 2017). However, PMIP3 simulations underestimated the proxy-based reconstructed LIG temperature response. For example, climate reconstructions suggest that the maximum temperature during the early LIG (before 126 ka BP) was about 2–5 °C higher than the pre-industrial in the mid- and high latitudes of the NH (CAPE Last Interglacial Project Members, 2006; Turney and Jones, 2010; McKay et al., 2011; Sanchez-Goni et al., 2012). Ensembles of climate models simulations underestimated the magnitude of this warming by several degrees (Braconnot et al., 2012; Masson-Delmotte et al., 2013; Lunt et al., 2013; Otto-Bliesner et al., 2013). In their simulations, the full magnitude of the reconstructed NH annual warming is only reached in summer (Lunt et al., 2013; IPCC, 2013; Otto-Bliesner et al., 2013). In addition, the mismatches point of model-data comparisons also calls for further study of the sensitivity of the simulations to uncertainties in the specified boundary conditions, although the lig127 k model ensemble in PMIP4 indicates good agreement with data reconstructions for summer temperature anomalies over Canada, Scandinavia, and the North Atlantic (Otto-Bliesner et al., 2019).

One potential reason for these discrepancies is the prescribed pre-industrial vegetation in these LIG simulations, which excluded dynamical vegetation impacts on climate. Dynamical vegetation interacts with the atmosphere at both regional and global scales through changes in albedo and soil moisture (biogeophysical feedbacks) and changes in carbon and other nutrient cycles (biogeochemical feedbacks; Claussen, 2009). Positive vegetation-albedo feedbacks were suggested by a few LIG simulation studies including dynamical vegetation (Calov et al., 2005; Crucifix and Loutre, 2002; Fischer et al., 2010; Gröger et al., 2007; Petoukhov et al., 2000; Schurgers et al., 2006, 2007). For example, a vegetated Sahara during the early LIG can cause as much as 20% local surface albedo changes and more than 10% increase in global latent heat loss when compared to pre-industrial desert (Schurgers et al., 2007). Moreover, due to the positive vegetation feedback during the early LIG, precipitation is increasing up to a doubling in a vegetated Sahara state compared to a prescribed desertic Sahara (Gröger et al., 2007). However, these vegetation feedbacks are not included in PMIP3. Thus, a complete estimation of impacts of vegetation feedbacks on the LIG climate allows us to explain the model-data discrepancies in terms of dynamic vegetation and enhances the robustness of the LIG simulations in the ongoing new phase of PMIP (PMIP4; Otto-Bliesner et al., 2017).

The Sahara, the largest tropical desert, was much greener and moister than today during the LIG (Rohling et al., 2002; Osborne et al., 2008; Fleitmann et al., 2011) and the early-to-mid-Holocene (Jolly et al., 1998; Hoelzmann et al., 1998; Prentice et al., 2000). During the LIG, the changing of moist and green North Africa to desert is suggested have influence on dispersal of early humans through expansions and contractions of well-water corridors (Kutzbach et al., 2020). In the Holocene, this phase of a green and moist Sahara is referred to as the African Humid Period (AHP). During the AHP, high precipitation related to strong summer monsoons promoted grass expansion in northern Africa, inducing a lower surface albedo and higher evaporation compared to desert (Hoelzmann et al., 1998). Around 5 ka BP, the orbitally-forced decrease in summer insolation led to the termination of this AHP, resulting in North African desertification (Charney, 1975; Claussen and Gayler, 1997; Claussen et al., 1999; Renssen et al., 2003; Liu et al., 2006; Notaro et al., 2008; Timm et al., 2010). This desertification triggered a regional increase in surface pressure suppressing convective precipitation. A weakening of the trade winds, the westerlies and the polar easterlies then followed the increased surface pressure. As a final result, desertification promoted a reduced meridional heat transport by the atmosphere from low latitudes to the Arctic, contributing to high-latitude cooling (Davies et al., 2015; Muschitiello et al., 2015). Theoretically, compared to the Holocene, a similar sequence of events, only with stronger amplitudes can be expected during the LIG due to the larger amplitude of the LIG insolation changes. However, the magnitudes of these regional vegetation feedbacks (in particular the impact of vegetated Sahara on climate during the LIG) and long-range effects through teleconnections have not yet been studied in detail.

In this study, we therefore designed a series of model experiments to assess the evolution of vegetation during the LIG and the magnitude of dynamical vegetation feedbacks. Our experiments were performed using the iLOVECLIM climate model, in which one of two vegetation models with differing complexity (VECODE and LPJ-GUESS) were coupled separately. The use of two vegetation models increases our insight into the model-dependency of the simulation results. During these simulations, VECODE was synchronously coupled, while LPJ-GUESS was asynchronously coupled to iLOVECLIM. We focus on the impacts of dynamic vegetation on the early LIG climate simulations and biogeophysical effects of vegetated Sahara on the LIG climate on both regional and global scales. The following questions will be addressed:

1) How abrupt is the 'green-to-desert' vegetation transition in the Sahara during the LIG?
2) What is the magnitude of dynamic vegetation feedbacks during the LIG?
3) To what extent are discrepancies between reconstructions and simulations related to vegetation feedbacks in the Sahara?

2. Methods

2.1. Model descriptions

2.1.1. The iLOVECLIM climate model

We applied the climate model iLOVECLIM version 1.0, which is an updated version of LOVECLIM 1.2 (Goosse et al., 2010; Roche et al., 2014). This intermediate complexity model includes the main climatic system components, e.g., atmosphere (ECBilt), oceans (CLIO), and vegetation (VECODE). Previously, this model has been successfully applied to analyze climate-vegetation interactions during the Holocene AHP (Renssen et al., 2003, 2006). In the present study, we apply three model configurations: (1) ECBilt-CLIO fully-coupled to the vegetation model VECODE (ECBilt-CLIO-VECODE); (2) ECBilt-CLIO asynchronously-coupled to the vegetation model LPJ-GUESS (ECBilt-CLIO_LPJ-GUESS); and (3) ECBilt-CLIO with prescribed pre-industrial vegetation obtained from Land-Use Harmonization (LUH2, 2012) (ECBilt-CLIO-LUH2). The LUH2 (Land-Use Harmonization, Phase 2) project prepared a harmonized set of land-use scenarios that smoothly connects the

historical reconstructions of land-use with the future projections in the format required for Earth System Models (LUH2, 2012). We applied the land-use data from the CMIP LUH2 dataset, at 850 AD. ECBilt is a three-level quasi-geostrophic atmospheric model at T21 resolution (Opsteegh et al., 1998). It provides the climate input for a vegetation component (VECODE, LPJ-GUESS), consisting of annual mean temperature, precipitation and GDD0 (growing degree days above 0 °C) for VECODE and monthly mean temperature, precipitation and cloud cover for LPJ-GUESS at the nominal T21 resolution. CLIO consists of a three-dimensional, free-surface ocean general circulation model coupled to a dynamic-thermodynamic sea-ice model (Goosse et al., 2010). This oceanic component has a horizontal resolution of 3° latitude by 3° longitude, and 20 unevenly spaced vertical layers in the ocean.

The difference among these three model configurations is their vegetation component and thereby the surface albedo and soil moisture. In the fully-coupled version, VECODE calculates covers of two Plant Functional Types (PFTs, grasses and trees), and bare soil as a dummy type, at an annual time step (Brovkin et al., 1997). VECODE calculates dynamic vegetation depending on bioclimatic constraints from ECBilt with the same spatial resolution. Soil hydrology is computed in a simple bucket model (LBM) embedded in ECBilt, in which the maximum water volume of the bucket is a function of vegetation cover. Likewise, soil hydrology is also relies on the LBM in the asynchronously-coupled version, although there is a full hydrology model in LPJ-GUESS since the water exchanges in LPJ-GUESS are only connected to the precipitation input provided by ECBilt but not used in the asynchronous coupling of ECBilt-CLIO to LPJ-GUESS. In the fully- and asynchronously-coupled versions of iLOVECLIM (ECBilt-CLIO-VECODE and ECBilt-CLIO_LPJ-GUESS), surface albedo is calculated in ECBilt based on dynamical vegetation cover in either VECODE or LPJ-GUESS. In contrast, in the version with prescribed vegetation (ECBilt-CLIO-LUH2), the land surface albedo is spatially varying, but is seasonally fixed in time at a constant value. Similar to both the fully- and asynchronously-coupled versions, soil hydrology in the version (ECBilt-CLIO-LUH2) is also decided in the simple bucket model in ECBilt, and the size of the bucket is fixed as a function of the prescribed pre-industrial vegetation cover.

2.1.2. The LPJ-GUESS vegetation model

LPJ-GUESS (V3.1) is a process-based dynamical vegetation model (Smith et al., 2001, 2014). The model employs biophysical and physiological process parameterizations identical to the equilibrium model BIOME3 (Haxeltine and Prentice, 1996). Vegetation dynamics in the model result from growth and competitions for light, space and soil resources among 11 plant functional types (PFTs) in each of several patches (15 patches in this study) for each simulated grid cell. A patch represents the vegetation distribution as a result of vegetation stands succession, corresponding to the maximum influencing area of one large full-grown individual (trees in most cases) on its neighbors. Physiological processes are simulated with a daily time step. The net primary production (NPP) is accrued at the end of a simulation year (Smith et al., 2001), resulting in changes in height, diameter and biomass growth of each PFT.

LPJ-GUESS requires monthly temperature, precipitation, cloud cover and CO_2 concentration as input. Since cloud cover is prescribed in iLOVECLIM, the transient climatic forcing of LPJ-GUESS only consists of varying temperature and precipitation. In this study, the model is asynchronously coupled to iLOVECLIM. In this asynchronous coupling procedure (Fig. 1), monthly climate inputs from the fully coupled iLOVECLIM model (ECBilt-CLIO-VECODE) are in an initial step fed to LPJ-GUESS, which simulates vegetation distributions. Then, the resulting vegetation distributions are given back to ECBilt, as a fixed vegetation component in iLOVECLIM (ECBilt-CLIO_LPJ-GUESS) during the next round of climate simulation. A new climatology from this integration is simulated and, subsequently, used off-line as climate forcing by LPJ-GUESS to produce a new global vegetation distribution that is subsequently used as a boundary conditions by iLOVECLIM, and so on. This sequence of simulating vegetation from climatological forcing, integrating the vegetation change into the climate model and computing vegetation distributions from it is referred to as an 'iteration'. Several iterations are performed until the vegetation distributions and climate states of successive iterations do not reveal any significant trend. Previously, the frequency of this type of iteration was tested with the climate model ECHAM and the BIOME vegetation model by Claussen (1994). He suggested that there is no significant difference between vegetation and climate patterns with an iteration frequency of five or ten years. In his study, most vegetation changes occur at the first iteration in the pre-industrial experiments, but it takes 3 iterations for the combined climate model to approach a new equilibrium state after a strong perturbation. Shortly thereafter, Claussen (1997) successfully applied this asynchronous coupling approach (four iterations with a frequency of five years) to analyze vegetation feedback in the African and Indian monsoon region. As reported in the supplementary information, we have also tested the suitability of these frequencies in our study. A frequency of 10 years is chosen, and four iterations are performed for the asynchronous couplings with this frequency. We treated vegetation results from the last iteration as vegetation responses to climate during the LIG and analyze vegetation feedbacks to climate. Our tests show that, using this asynchronous coupling, the climate is able to adjust to the vegetation computed by LPJ-GUESS.

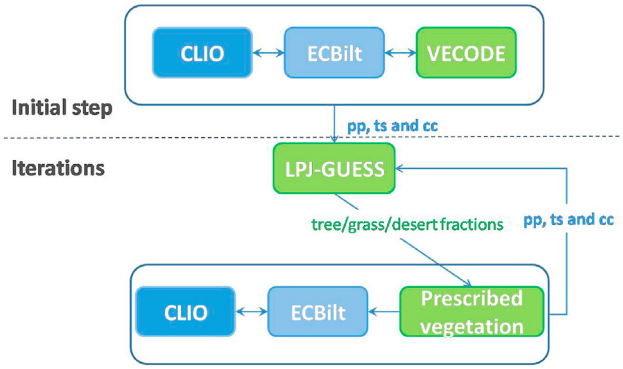

Fig. 1. Schematic illustrating the asynchronous coupling process. CLIO = ocean, ECBilt = atmosphere, VECODE or LPJ-GUESS = vegetation; pp = monthly mean precipitation, ts = monthly mean surface temperature, and cc = monthly mean cloud cover. In the initial step, monthly climate inputs from the fully coupled iLOVECLIM model (ECBilt-CLIO-VECODE) are fed to LPJ-GUESS, which simulates vegetation distributions. Then, during the iterations, the resulting vegetation distributions are given back to iLOVECLIM (ECBilt-CLIO-prescribed vegetation) as the prescribed vegetation components during the next round of climate simulation.

2.2. Experimental design

We performed three types of experiments (Table 1): 1, experiments with fixed pre-industrial forcings, 2, experiments with transient last interglacial forcings and 3, sensitivity experiments. For type 1, three experiments are performed with iLOVECLIM with fixed pre-industrial vegetation, namely obtained from fully coupled VECODE (**PI_VEC**), asynchronously coupled LPJ-GUESS (**PI_LPJ**), and observations by LUH2 (2012) (**PI_FIX**). The goal of these type 1 experiments is to provide pre-industrial references for the LIG

Table 1
Overview of the experiments.

PI_VEC	Pre-industrial run with dynamical vegetation in VECODE (ECBilt-CLIO-VECODE)		
PI_FIX	Pre-industrial run with fixed vegetation from **CMIP LUH2** (ECBilt-CLIO-LUH2)		
PI_LPJ	Pre-industrial run with **asynchronously** dynamical vegetation in **LPJ-GUESS** (ECBilt-CLIO-LPJ-GUESS)		
127K_VEC	127ka BP ctrl run with dynamical vegetation in **VECODE** (ECBilt-CLIO-VECODE)		
LIG_VEC	The LIG (127ka BP- 116ka BP) run with transient insolation forcing and dynamical vegetation in **VECODE** (ECBilt-CLIO-VECODE)		
LIG_FIX	The LIG (127ka BP- 116ka BP) run with transient insolation forcing and fixed vegetation from **CMIP LUH2** (ECBilt-CLIO-LUH2)		
LIG_LPJ	The LIG (125ka BP- 117ka BP) run with 1ka interval insolation forcing and asynchronously dynamical vegetation in **LPJ-GUESS** (ECBilt-CLIO-LPJ-GUESS)		
S125K_NA$_{VEC}$	Sensitivity run with insolation forcing in 125ka BP and fixed vegetation	The fixed vegetation is a combination of **pre-industrial vegetation from CMIP LUH2** and **125ka BP North African vegetation (15–30N, 10W-35E)** from:	**51% grass cover + 14% tree cover**
S125K_NA$_{LPJ}$			**75% grass cover**
S125K_NA$_{GRASS}$			**100% grass cover**
S125K_NA$_{PI}$		The fixed vegetation is from:	**0%**

experiments. For type 2, two transient LIG (127 ka BP - 116 ka BP) simulations are performed, either with fully coupled dynamical vegetation using VECODE (**LIG_VEC**) or with fixed pre-industrial vegetation from CMIP LUH2 (**LIG_FIX**). These two LIG simulations start from the same equilibrium experiment 127 K_VEC. In addition to these two long runs, LIG simulations (**LIG_LPJ)** with dynamical vegetation are performed with LPJ-GUESS asynchronously coupled to iLOVECLIM, covering 125 ka BP to 117 ka BP at 1 ka intervals. For each 1 ka experiment of LIG_LPJ, LPJ-GUESS is forced by initial climate forcing from LIG_VEC, and then the asynchronous coupling (Section 2.1.2) starts with vegetation from LPJ-GUESS. Besides type 1 and 2 experiments, four sensitivity experiments (type 3) are performed, all with identical insolation forcing at 125 ka BP, but with different fixed vegetation conditions. The goal of these sensitivity experiments is to investigate the regional and global impacts of the early LIG North African vegetation feedbacks on climate simulations. The fixed vegetation conditions are combinations of prescribed North African vegetation (15–30°N, 10°W-35°E) and pre-industrial vegetation in other regions. The pre-industrial vegetation is from the LUH2 dataset (LUH2, 2012). The four prescribed North African vegetation cover are from S125K_NA$_{VEC}$, S125K_NA$_{LPJ}$, S125K_NA$_{GRASS}$, and S125K_NA$_{PI}$, respectively.

The transient forcings (Fig. 2) for the last interglacial experiments (type 2) include the amount of insolation received by the Earth and greenhouse gases (GHG) concentrations. These forcings are identical to the PMIP4 protocol (Otto-Bliesner et al., 2017, PMIP4, 2017). Changes in insolation received by the Earth are calculated in iLOVECLIM during transient simulations according to Berger (1978). From 127 ka BP to about 119 ka BP, the NH received more insolation during boreal summer and less insolation during boreal fall and winter compared to preindustrial values. The GHG forcings for both transient experiments follow the PMIP4 protocol (PMIP, 2017) and are based on ice-core data from EPICA Dome C (Bereiter et al., 2015; Schneider et al., 2013) for CO_2, EPICA Dome C and EPICA Dronning Maud Land (Loulerge et al., 2008; Schilt et al., 2010a) for CH_4, as well as from EPICA Dome C and Talos Dome

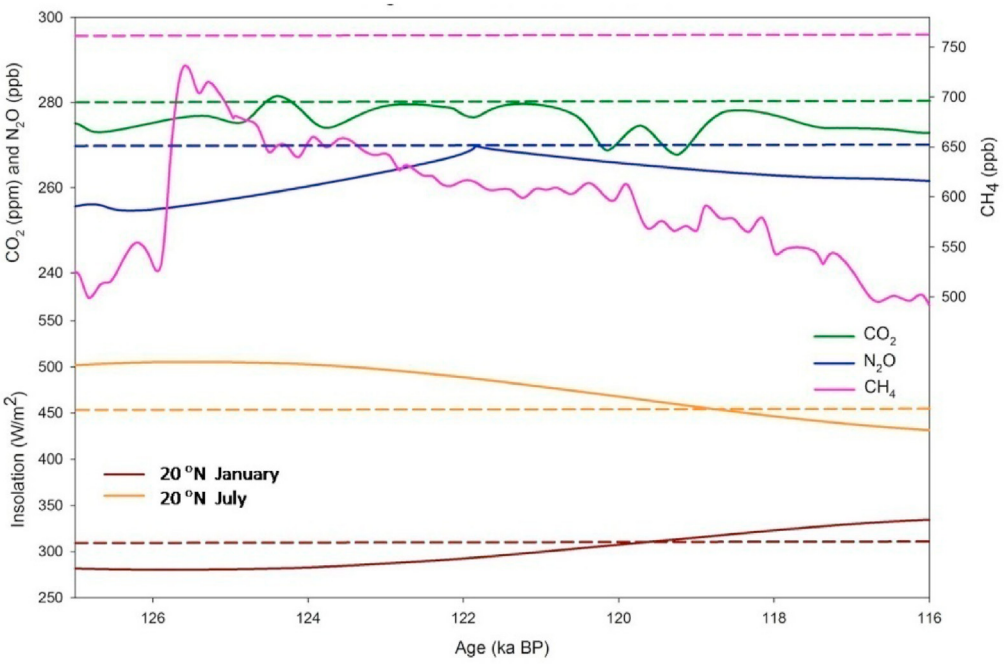

Fig. 2. Forcing of the LIG climate simulations over the period 127–116 ka BP. Greenhouse gas concentrations are according to the PMIP4 protocol (https://pmip4.lsce.ipsl.fr/doku.php/data:gases#schilt_et_al_n20_data), which is based on the ice-core data of Bereiter et al. (2015), Loulergue et al. (2008) and Schilt et al. (2010) for CO_2 (green lines), CH_4 (pink lines) and N_2O (blue lines), respectively, in the upper part of the figure. In the lower part of the figure, the January (brown lines) and July (yellow lines) insolation for 20°N are given (Berger, 1978). The corresponding pre-industrial values are given by the dashed lines. (For interpretation of the references to color in this figure legend, the reader is referred to the Web version of this article.)

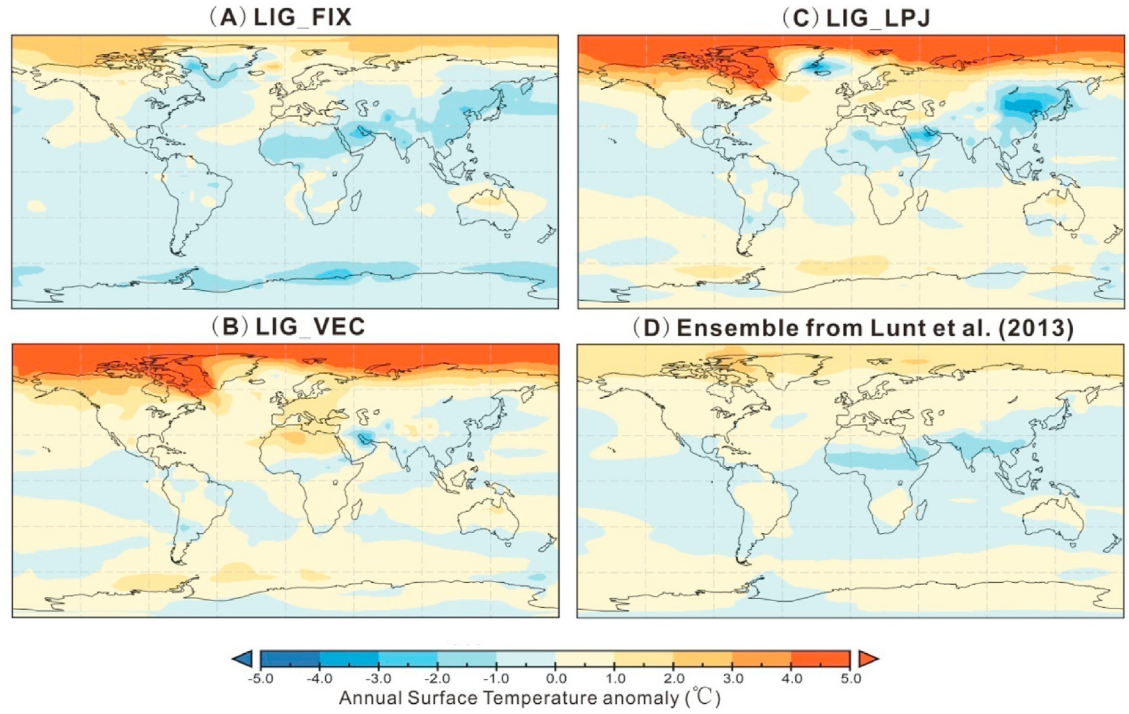

Fig. 3. Simulated surface temperature anomalies, LIG (125 ka BP) minus pre-industrial. a) LIG_FIX, b) LIG_VEC; c) LIG_LPJ and d) Ensemble mean of Lunt et al. (2013).

(Schilt et al., 2010a, b) for N_2O. A linear interpolation was applied to these data in order to get annual values for transient simulations. In contrast, the GHG levels are 100-year mean values of the linear interpolation for asynchronous coupled simulations, e.g., mean values from 124.95 ka BP to 125.05 ka BP for the simulation LIG_LPJ in 125 ka BP. For four sensitivity experiments (type 3), identical 125 ka BP orbital and GHG forcings (Fig. 2) are applied. The prescribed pre-industrial vegetation distribution is derived from LUH2 (2012), and represents conditions taken at 850 AD.

3. Results and discussions

3.1. Global temperature trends and vegetation effects

Compared to pre-industrial conditions, the simulated early LIG (125 ka BP) in LIG_FIX suggests maximum annual warming at high latitudes and little temperature changes in the tropics except for the Indian and African monsoon regions where temperatures are lower (Fig. 3a). These main features are in good agreement with the simulated multi-model mean (Fig. 3d) reported by Lunt et al. (2013) and IPCC (2013) in which vegetation is also fixed at a pre-industrial level. As expected, similar to Lunt et al. (2013), our simulation LIG_FIX underestimates the proxy-based evidence (Turney and Jones, 2010; McKay et al., 2011) for warming of the far northern coastal regions of Alaska (simulated 0–1 °C versus data 5.5–6 °C) and Siberia (simulated 0–1 °C versus data 7.1–14.8 °C). In contrast, simulation LIG_VEC (Fig. 3b) and LIG_LPJ (Fig. 3c) suggest slightly better agreements with proxy data than LIG_FIX, with 1–2 °C warming in coastal regions of Alaska and Siberia, respectively. In addition, the strong warming over Northern Hemisphere in LIG_FIX is consistent with the CMIP6-PMIP4 lig127 k simulations (Otto-Bliesner et al., 2019). Besides the high-latitude regions, simulation LIG_VEC and LIG_LPJ also suggest a 0–1 °C warming in the tropics (30°S-30°N), in particular in North Africa (with a maximum of warming by about 3 °C). This tropical warming agrees with the 0.3 °C warming suggested by proxy data (Turney and Jones, 2010; McKay et al., 2011).

The stronger temperature response in LIG_VEC and LIG_LPJ compared to LIG_FIX highlights the importance of vegetation impacts on the high latitudes and tropical regions, where the 125 ka BP vegetation is significantly different in these two sets of simulations. In most boreal regions, trees extend further north and tree cover is higher by up to 50% at 125 ka BP compared to pre-industrial conditions (Fig. 4b and c). The higher tree cover indicates a lower surface albedo compared to snow-covered tundra in these regions, leading to an increase in absorbed shortwave radiation, resulting in a positive surface temperature anomaly (>2.5 °C) simulated in LIG_VEC and LIG_LPJ. Likewise, in North Africa where the vegetation cover in LIG_VEC and LIG_LPJ is larger than LIG_FIX, positive surface temperature anomalies (~1.5 °C) are shown in both simulations, notably in the northwestern part of this region (Fig. 3b and c). At 125 ka BP, the total precipitation in North Africa is about 60 cm/yr and 58 cm/yr in LIG_VEC and LIG_LPJ, respectively. These amounts of precipitation are more than double those from LIG_FIX (about 28 cm/yr at 125 ka BP). This magnitude of vegetation feedback to precipitation in North Africa lies in the same range as simulated by Gröger et al. (2007) and Schurgers et al. (2006), who simulated amplifications by a factor 2 and 3, respectively.

Following Bakker et al. (2014), we quantified the linear annual mean temperature trends (AMTT) per latitude, over an interval from 123 ka BP to 116.2 ka BP. In our LIG transient simulations (LIG_FIX and LIG_VEC), the AMTTs show distinct latitudinal dependencies (Fig. 5a), in particular in LIG_FIX, with a strong negative trend at high-latitudes, a less negative trend at mid-latitudes, and a slight positive trend at low-latitudes. Compared to AMTT in LIG_FIX, LIG_VEC suggests a better agreement with reconstructions. The AMTTs in LIG_FIX are −0.9 °C/ka at northern high latitudes. In contrast, the AMTTs at southern high latitudes and at latitudes between 10°N and 40°N indicate insignificantly negative and positive trends in LIG_FIX, respectively. These simulated AMTTs in

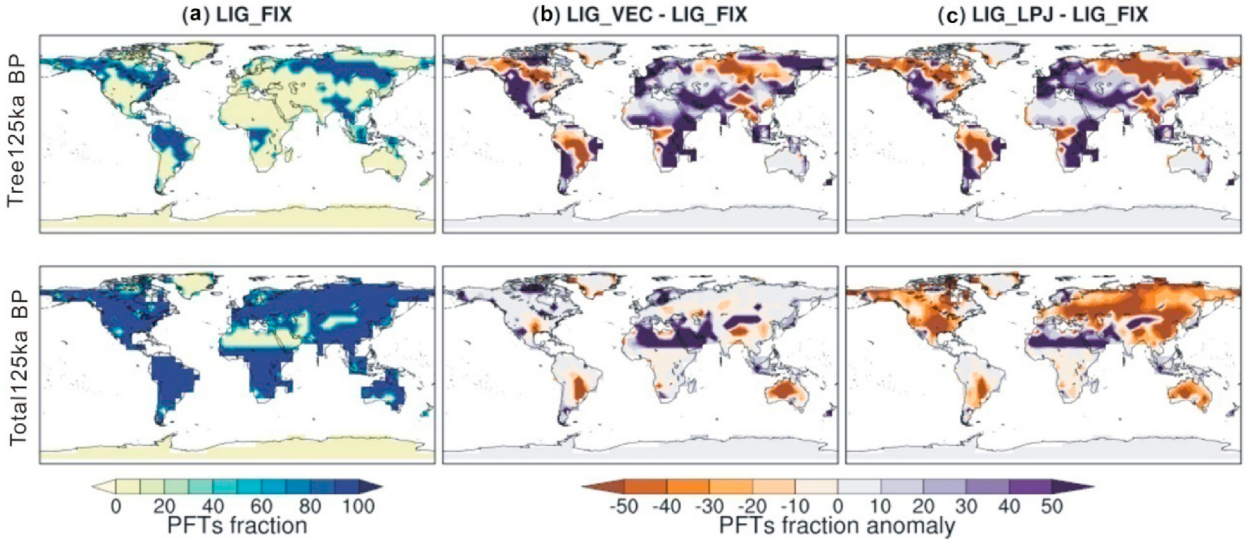

Fig. 4. Vegetation (tree and total) cover under pre-industrial condition in LIG_FIX (a) and 125 ka BP vegetation anomalies simulated by VECODE (b), as indicated by the LIG_VEC minus LIG_FIX anomaly, and by LPJ-GUESS(c), as indicated by the LIG_LPJ minus LIG_FIX anomaly.

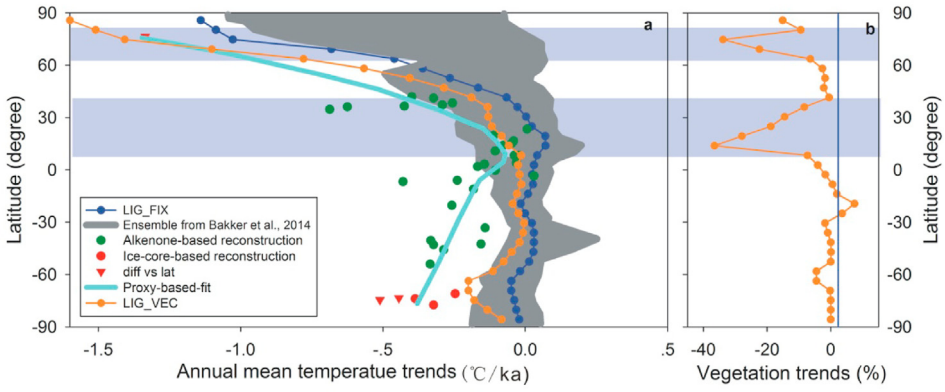

Fig. 5. Latitudinal LIG annual mean temperature trends (AMTT, a) in model and data (Bakker et al., 2014). The blue and orange lines are 50 years mean latitudinal LIG AMTT from LIG_FIX and LIG_VEC, respectively. The grey shading represents the maximum and minimum trends among multi-model simulations (Bakker et al., 2014). The red and green dots are AMTT based on the Greenland and Antarctic ice-cores and alkenone. The cyan line shows both proxies based AMTT fit, indicating the general latitudinal trends. The right panel (b) indicates vegetation trends anomaly compared to fixed pre-industrial level (total vegetation cover changes from 123 ka BP to 116.2 ka BP) in LIG_VEC. The light blue bands indicate the latitudes where experience strong vegetation changes during the specific period. (For interpretation of the references to color in this figure legend, the reader is referred to the Web version of this article.)

LIG_FIX are consistent with multi-model simulations in Bakker et al. (2014). In their study, the multi-model simulations include seven models in which pre-industrial vegetation is prescribed and two models in which dynamical vegetation modules (CLIMBER-2 and MPI-UW) are included. Interestingly, although these two models simulate rather different July temperatures at northern high latitudes and tropics compared to the other seven LIG simulations (Bakker et al., 2013; Schurgers et al., 2007), the AMTTs in the two models do not lie outside the range of the other simulations in these specific regions. In contrast, the AMTT in LIG_VEC is not only stronger than the AMTT in LIG_FIX at all latitudes, but also lies outside the range of AMTTs in Bakker et al. (2014) at high latitudes (Fig. 5a). LIG_VEC indicates stronger AMTTs by −0.4 °C/ka and −0.2 °C/ka compared to LIG-FIX at northern and southern high latitudes, respectively. In addition, a stronger negative AMTT of −0.1 °C/ka is shown in LIG_VEC at latitudes between 10°N and 40°N. These stronger AMTTs in LIG_VEC are positively correlated to the total vegetation cover trends (Fig. 5b), implying positive vegetation impacts on temperature at a global scale. Even so, the AMTT in LIG_VEC is still smaller than the reconstructed value: Greenland (−1.5 °C/ka), the northern mid-latitudes (−0.5 °C/ka), low-latitudes (−0.2 °C/ka) and the southern mid-to high-latitudes (−0.3 °C/ka).

3.2. Vegetation evolution and its local effects in the Sahara

During the LIG, the Sahara is the region with strongest changes in vegetation, with a reduction of total vegetation cover from more than 70% at 125 ka BP to only about 10% at 117 ka BP in both LIG_VEC and LIG_LPJ (Fig. 6a–c). Based on the vegetation change rates (Fig. 6d–f), we describe the local effects of these vegetation changes on climate in three phases. They are the green Sahara phase in the early LIG, the termination phase of the LIG AHP and the last phase of the LIG. We defined the impacts of the vegetation feedbacks by calculating the differences in climate features (such as temperature, precipitation) between LIG_VEC/LIG_LPJ and LIG_FIX,

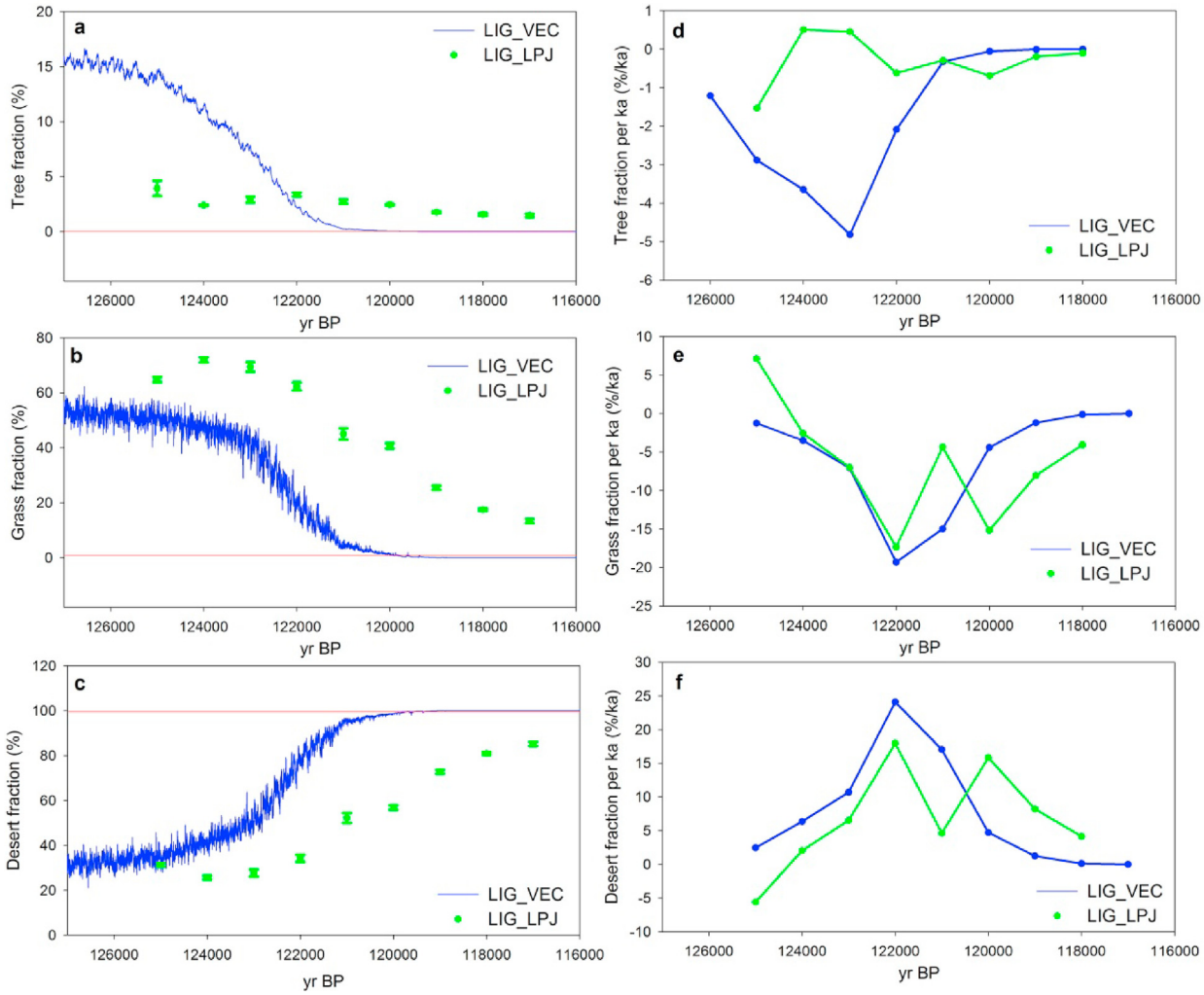

Fig. 6. Vegetation covers (tree (a), grass (b) and desert (c)) evolution and their changing rates (tree (d), grass (e) and desert (f) from 127 ka BP to 116 ka BP over Sahara. The red line indicates LIG_FIX values; the blue line indicates LIG_VEC results; and the green circles indicate LIG_LPJ results. (For interpretation of the references to color in this figure legend, the reader is referred to the Web version of this article.)

and hereafter we refer to these impacts as "vegetation feedbacks".

3.2.1. Early LIG (green Sahara)

During the early LIG (from 127 ka BP to about 123 ka BP), vegetation is dominated by grass and total vegetation cover stabilizes at a relatively high level (about 70%) in both LIG_VEC and LIG_LPJ (Fig. 6a–c). In this phase, the orbitally-forced insolation (Fig. 2) remains at a relative high level (around 500 W/m^2 at 20°N in July), heating the land surface in summer and thereby enhancing the atmospheric monsoonal moisture transport. Without dynamical vegetation (LIG_FIX), about 26 cm/yr precipitation is simulated during this phase over the Sahara. In the simulations with dynamical vegetation (LIG_VEC and LIG_LPJ), the precipitation values for the Sahara are about twice as high (~60 cm/yr, Fig. 7a) as those in LIG_FIX, the mean surface temperature being also higher (31.5 °C in LIG_VEC and LIG_LPJ vs. 29.0 °C in LIG_FIX, Fig. 7b). In LIG_VEC and LIG_LPJ, the vegetation cover is enhanced by these relatively large amounts of precipitation and high surface temperatures. The high vegetation cover modelled in LIG_VEC and LIG_LPJ are in agreement with reconstructed dominant vegetation of wooded grassland by Larrasoana et al. (2013) under precipitation ranging from 26.5 cm/yr to 125.5 cm/yr across tropical Africa.

The only difference in simulation setup between LIG_VEC/LIG_LPJ and LIG_FIX is the presence of a dynamical vegetation model to which we attribute the higher amount of precipitation and surface temperatures. Compared to the prescribed pre-industrial vegetation (desert) in LIG_FIX (Fig. 4), the lower albedo of grass (0.20 versus 0.33 for desert) in LIG_VEC and LIG_LPJ results in a lower reflection of incoming shortwave radiation, an increase in net radiation, and therefore higher surface temperature (2.5 °C) over land. Compared to LIG_FIX, the enhanced land-sea thermal contrast and declines of the surface pressure over land is indicated in both LIG_VEC and LIG_LPJ (Fig. 3), thereby leading to increased moisture transport from the tropical oceans into North Africa and more precipitation (Charney, 1975; Eltahir, 1996; Eltahir and Gong, 1996; Braconnot et al., 1999; Schurgers et al., 2006). Besides these two vegetation effects on climate (higher temperature and precipitation), vegetation further enhances precipitation by promoting the local soil moisture content (Fig. 7c) and thereby evaporation (Fig. 7d), thus enhancing the local hydrological circulation. Therefore, the vegetation feedback on precipitation peaks in this green Sahara phase, corresponding to the largest contrast in vegetation (grass vs. desert) compared to LIG_FIX (Figs. 6 and 8). Similar magnitudes of feedback to precipitation were suggested by previous studies (Gröger et al., 2007; Schurgers et al., 2007), although the vegetation feedbacks were investigated for slightly different

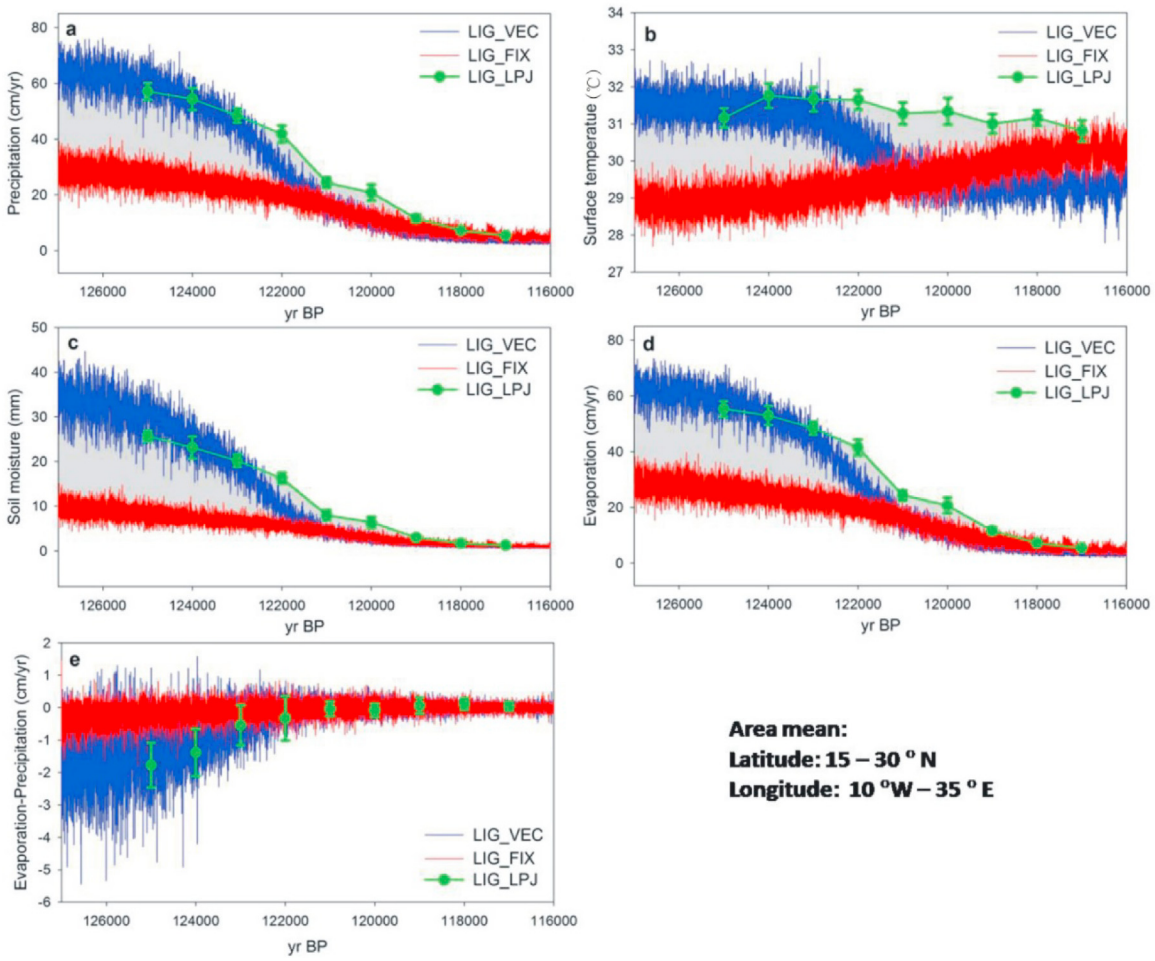

Fig. 7. Time series (127 ka BP - 116 ka BP) of (a) precipitation, (b) temperature, (c) soil moisture, (d) surface evaporation and (e) values of evaporation minus precipitation over the Sahara; the blue and red lines indicate LIG_VEC and LIG_FIX results, respectively; the green circles with error bar indicate results of LIG_LPJ. The grey shading represents climate changes related to vegetation feedback. (For interpretation of the references to color in this figure legend, the reader is referred to the Web version of this article.)

area in North Africa (Fig. 9). Our study confirms the strong positive North African vegetation feedbacks to precipitation by a factor of 2–3 for the early LIG compared to the fixed pre-industrial LIG simulations.

3.2.2. *Desertification during the LIG*

Starting from 123 ka BP, vegetation cover (Fig. 6a–c) decreases largely in both LIG_VEC and LIG_LPJ, in combination with large declines in precipitation (Fig. 7a) and surface temperature (Fig. 7b). The rates of grass cover decrease (−18%/ka and −14%/ka) peak at 122 ka BP in both LIG_VEC and LIG_LPJ, while desert expands at rate of 25%/ka and 15%/ka, respectively (Fig. 6d–f). Moreover, the rates of vegetation changes in both LIG_VEC and LIG_LPJ are faster than the declines of summer insolation at 20°N, whose decline peaks by about 3.5% at around 120 ka BP. Total vegetation cover in LIG_VEC reaches a relatively low level at around 121 ka BP, which is earlier than in LIG_LPJ (around 119 ka BP). This difference in the timing of the desertification between LIG_VEC and LIG_LPJ could be a result of differences in model complexity. In the relatively complex LPJ-GUESS model, more gradual vegetation responses can be expected when more plant types interact with climate (Claussen et al., 2013; Hely et al., 2014; Li et al., 2019).

Corresponding to simulated vegetation changes in this phase, feedbacks to precipitation and soil moisture (Fig. 8a and c) experience a rapid reduction from 123 ka BP to 121 ka BP and becomes rather close to the LIG_FIX level at 119 ka BP. The impacts of these vegetation feedbacks are calculated based on climate anomalies between simulations LIG_VEC/LIG_LPJ and LIG_FIX (Fig. 8), and hereafter we refer to these impacts as “vegetation feedbacks”. In LIG_VEC, the vegetation feedback to precipitation (Fig. 8a) declines by 21 cm/yr from 123 ka BP to 121 ka BP, but with only <1 cm/yr after 121 ka BP. In LIG_LPJ, this feedback (Fig. 8a) also declines rapidly from 123 ka BP to 121 ka BP by 15 cm/yr, followed by a slower decline from 8 cm/yr to <1 cm/yr from 121 ka BP to 119 ka BP. In both LIG_VEC and LIG_LPJ, the feedbacks to precipitation and temperature (Fig. 8a and b) decline almost in phase with vegetation changes (Fig. 6b) and their declined rates peak at the period between 123 ka BP and 121 ka BP. The faster declines in vegetation feedbacks to precipitation (Fig. 9) than the early LIG are consistent with Gröger et al. (2007) and Schurgers et al. (2007). The feedback in LIG_LPJ is more close to their results than LIG_VEC, of which the magnitude declines more gradually from 123 ka BP to 119 ka BP. Due to the exchanges between latent and sensible heats and the spatial heterogeneity of temperature changes, there are slight increases in mean surface temperature in North Africa in LIG_FIX. The temperature feedback in LIG_LPJ keeps reducing gradually from 2.8 °C to 2.0 °C from 123 ka BP to 119 ka BP, while it drops from 2.5 °C to 0°Cand becomes slightly negative after 121 ka BP in LIG_VEC (Fig. 8b). Compared to the early LIG, the summer insolation (Fig. 8) also declines faster from 497 W/m^2 to 457 W/m^2 from 123

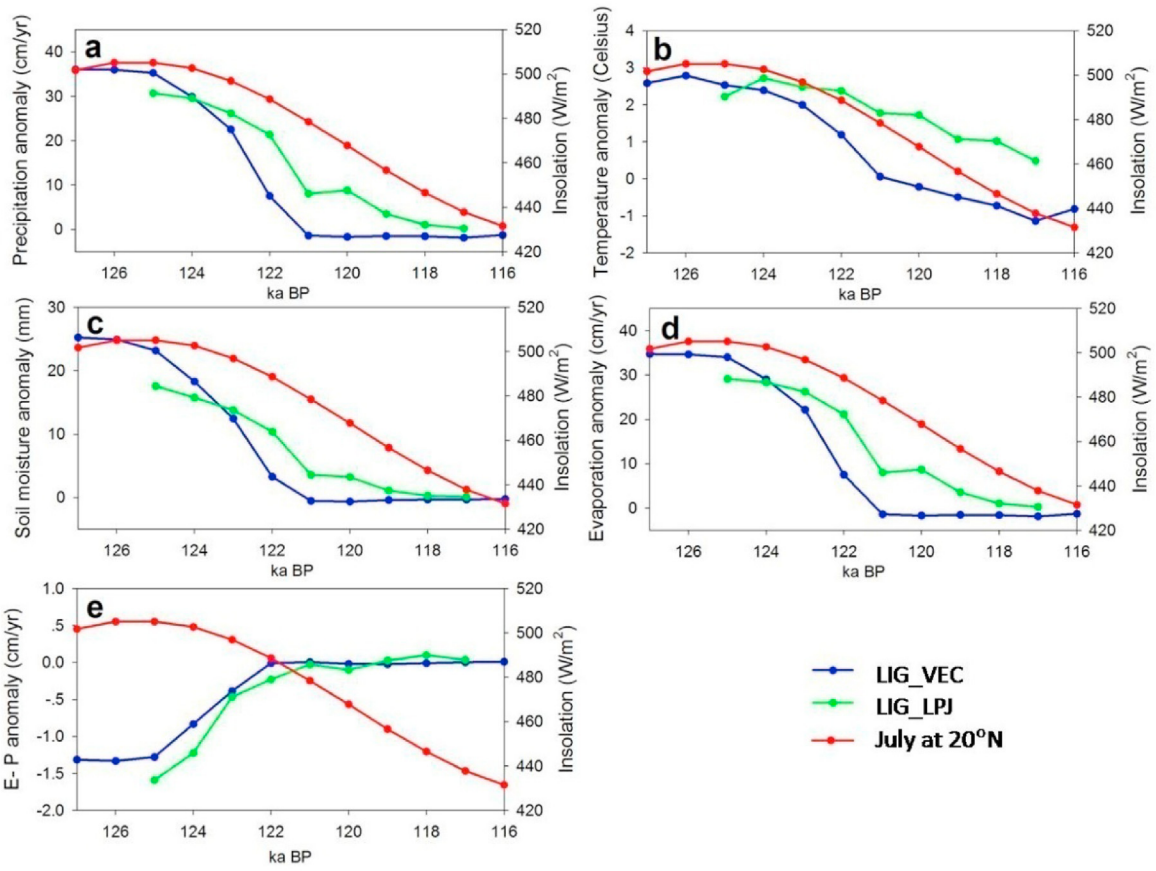

Fig. 8. Time series (127 ka BP - 116 ka BP) of biogeophysical vegetation feedbacks to (a) precipitation, (b) temperature, (c) soil moisture, (d) surface evaporation and (e) values of evaporation minus precipitation over the Sahara; the blue and green lines indicate feedbacks from LIG_VEC and LIG_FIX, respectively; the red lines indicate the main climate forcing (July insolation at 20°N). (For interpretation of the references to color in this figure legend, the reader is referred to the Web version of this article.)

ka BP to 119 ka BP, and the rate of this decline peaks between 121 ka BP and 119 ka BP. This decline in July insolation at 20°N dominates the fast reduction in vegetation cover at the beginning of the termination from 123 ka BP onwards, accelerating the AHP termination. Around this point, the magnitude of the positive vegetation feedbacks cannot offset the deficit due to decreased summer insolation.

3.2.3. *Last phase of LIG (desert)*

The vegetation cover (Fig. 6a–c) gradually decreases and reaches 0% in LIG_VEC after 121 ka BP, which is earlier than in LIG_LPJ. In contrast, vegetation cover decreases gradually from 25% to 12% in LIG_LPJ after the desertification at around 119 ka BP. The around 10% vegetation cover in LIG_LPJ and deserted Sahara in LIG_VEC are results of low precipitation in this region, which is consistent with reconstructions that is the <10% vegetation cover under precipitation between 10 cm/yr and 26.5 cm/yr (Larrasoana et al., 2013).

In the last phase of LIG, the magnitude of feedbacks (Fig. 8) is weaker than during earlier phases due to the lower vegetation cover, particularly in LIG_VEC. Less than 1 cm/yr precipitation anomaly (Fig. 8a) between LIG_VEC and LIG_FIX indicates the weak feedback to precipitation, while the precipitation anomaly in LIG_LPJ sees a gradual decline from 9 cm/yr at 121 ka BP to 2 cm/yr at 117 ka BP, corresponding to its vegetation cover. Similarly, a weak positive feedback to temperature (0.5 °C) remains in LIG_LPJ (Fig. 8b), which is a result of its slightly higher vegetation cover compared to LIG_FIX. However, the feedback to temperature in LIG_VEC (Fig. 8b) turns negative and reaches −0.8 °C, which could be related to the spatial heterogeneity of the dynamical vegetation which is different from the fixed pre-industrial vegetation.

3.3. *The global impacts of vegetation changes in Sahara*

The vegetated Sahara in the early LIG, as an important anomaly of global vegetation compared to pre-industrial vegetation, strengthens the warming at high latitudes through changes in the atmospheric circulation. The magnitudes of these teleconnected effects depend on the prescribed vegetation cover in sensitivity experiments (Table 1). Compared to the northern high latitudinal (>60°N) surface temperature in S125K_NA_{PI}, a warming of 1.25 °C is shown in S125K_NA_{GRASS} (Fig. 10c), which includes 100% grass cover in the Sahara. Weaker warming effects by about 1.0 °C (Fig. 10a, d) and 0.75 °C (Fig. 10b and e) are suggested in S125K_NA_{VEC} and S125K_NA_{LPJ}, respectively. The total vegetation cover in the Sahara is higher in S125K_NA_{LPJ} (about 75%) than in S125K_NA_{VEC} (about 65%). The stronger warming effect of vegetation feedback in S125K_NA_{VEC} than in S125K_NA_{LPJ} is related to the relatively higher tree cover in S125K_NA_{VEC} (Fig. 6), which has a lower albedo than grass (0.13 vs. 0.20). These results suggest that the contribution of Sahara vegetation feedbacks to high latitudinal temperature is positively related to Sahara vegetation cover, and explains about 30% of the simulated warming at high latitudes during the early LIG when taking into account global vegetation feedbacks (Fig. 10d and e).

Overall, these vegetated Sahara states in S125K_NA_{GRASS}, S125K_NA_{VEC} and S125K_NA_{LPJ} leads to a lower surface albedo than

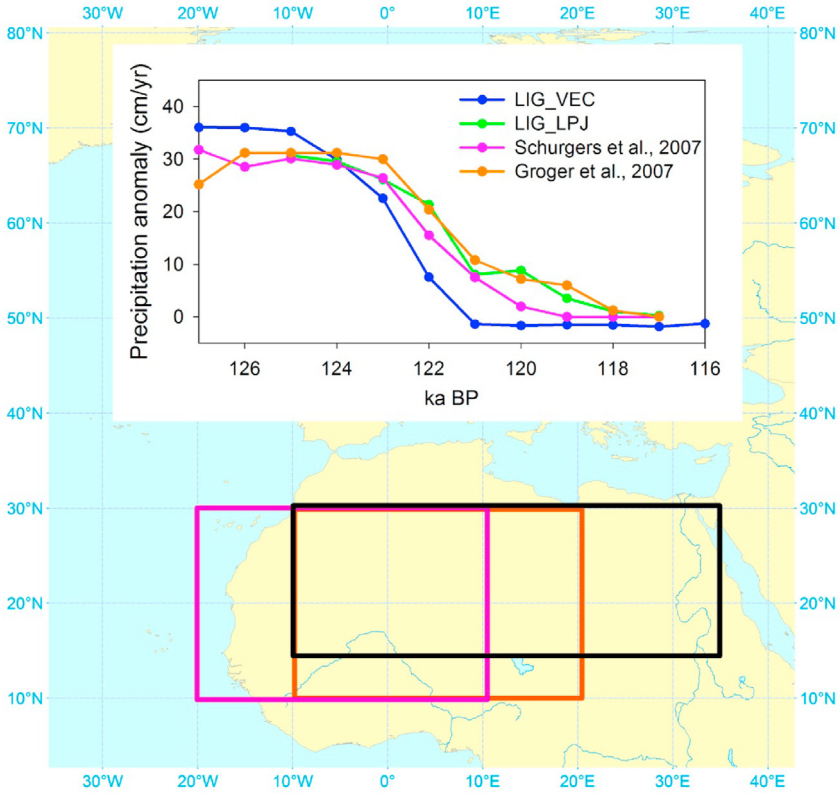

Fig. 9. Vegetation feedbacks to precipitation in North Africa during the LIG from different studies. (15–30°N, 10°W-35°E). The blue and green lines indicate feedbacks from LIG_VEC and LIG_FIX, respectively. The black box below shows the study area in both simulations. The pink line indicates results from Schurgers et al. (2007), and the orange line indicates results from Gröger et al. (2007). The boxes below indicate their study region, and the color is in line with the line plots. (For interpretation of the references to color in this figure legend, the reader is referred to the Web version of this article.)

the deserted Sahara in S125K_NA_{PI}, resulting in higher surface temperature, thereby causing a decline in surface pressure. Compared with S125K_NA_{PI} in 125 ka BP, the higher surface temperature in North Sahara and northern high latitudes and lower surface temperature in mid-latitudes in experiments with vegetated Sahara are similar to temperature patterns in 6 ka BP in Davies et al. (2015) and Muschitiello et al. (2015). As discussed by Davies et al. (2015) and Muschitiello et al. (2015) for the Holocene AHP, this decreased surface pressure then perturbs the extratropical atmospheric circulation. The perturbations enhance mid-latitude westerlies as a result of increased latitudinal temperature and pressure gradients, which then increase the amount of heat transported from tropical regions to the Arctic. These similar results for the LIG and the Holocene (e.g., Davies et al., 2015; Muschitiello et al., 2015), highlight the profound effects of North African vegetation changes on climate at global scale.

3.4. The uncertainties and outlook

The simplicity of the atmospheric component used impose several limitations. Indeed, ECBilt is based on a formulation of the quasi-geostrophic potential vorticity, and the ageostrophic terms are included as diagnostics based on the vertical velocity and the horizontal divergence (Opsteegh et al., 1998; Goosse et al., 2010). The simulation of the Hadley circulation is considerably improved but is still relatively poor compared to the mid- and high-latitudes when comparing with observations (Goosse et al., 2010). Moreover, a multi-model last interglacial study (Bakker and Renssen, 2014) suggests that EMICs often overestimate the maximum temperature at all latitudes compared to GCMs. We therefore recommend that the impacts of tropical vegetation cover changes on atmospheric circulations are further studied by involving fully coupled AOVGCMs and by repeating the simulations with a multi-model ensemble.

A second major source of uncertainty is related to the vegetation simulation which provides ECBilt with the land surface parameters (surface albedo and vegetation covers), resulting in vegetation feedbacks to climate. In our study, these land surface parameters are based on results from two vegetation models and are passed back to ECBilt through full- or asynchronous-coupling. VECODE, fully coupled to ECBilt, suggests dramatic North African vegetation change from 127 ka BP to 116 ka BP, leading to abrupt transition from green Sahara to desert. In contrast, LPJ-GUESS, asynchronously coupled to ECBilt, suggests a relatively gradual transition compared to fully coupled VECODE. One reason for this difference could be their difference in complexity. VECODE shows a more linear treatment of vegetation (i.e., either forest or desert combines with grass) compared to the more mixed PFTs compositions in LPJ-GUESS (Li et al., 2019). VECODE may therefore exaggerate vegetation responses to climate and thereby overemphasize impacts of vegetation on climate.

The more gradual vegetation responses to the LIG climate change in LPJ-GUESS compared to VECODE are consistent with an explanation that rather gradual vegetation responses to climate changes are simulated when all plant types interact with climate (Claussen et al., 2013; Hely et al., 2014). Due to the simple vegetation diversity in VECODE, the vegetation responses simulated in VECODE would represent the possible strongest vegetation changes during the LIG, and therefore indicate the possible largest vegetation feedbacks to climate. In contrast, the vegetation responses and

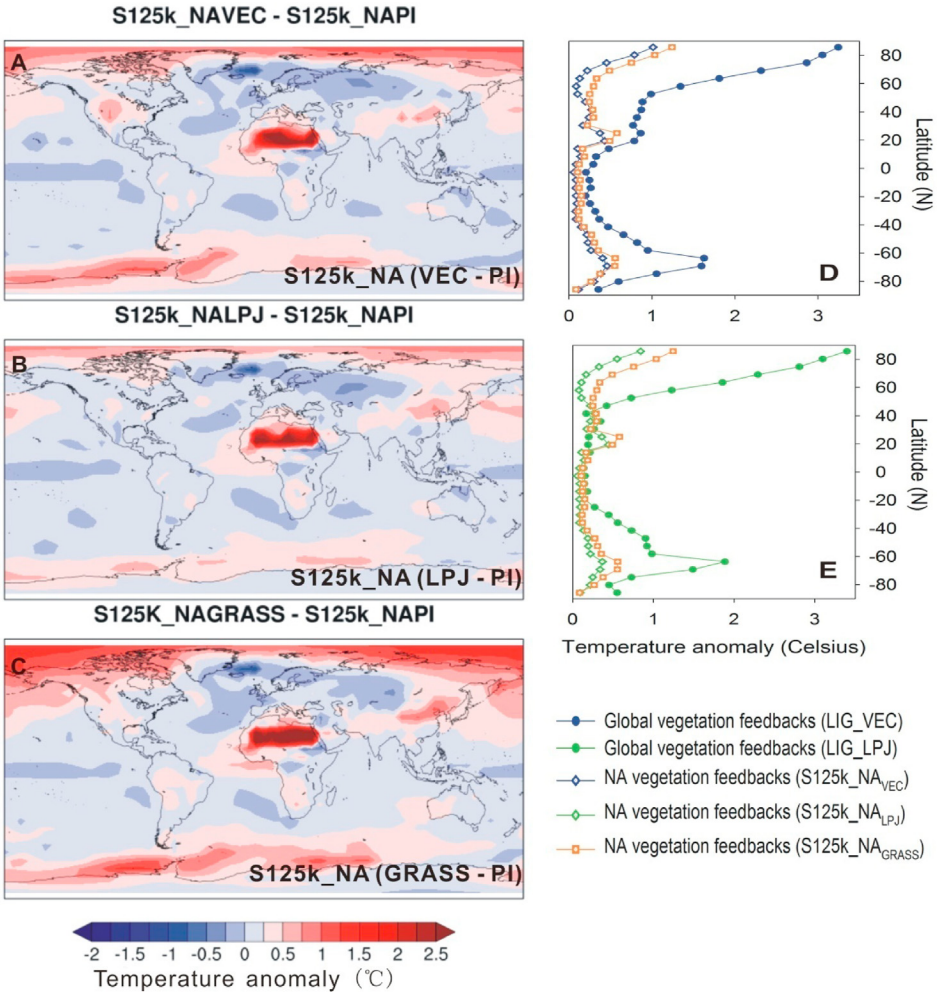

Fig. 10. 125 ka BP North African vegetation feedbacks on global surface temperature (ts) (the left side) and their latitudinal contributions compared to global vegetation feedbacks (the right side). On the left side, they are North Africa vegetation feedbacks in (a) S125K_NA$_{VEC}$, (b) S125K_NA$_{LPJ}$ and (c) S125K_NA$_{GRASS}$; on the right side, they are contributions of North Africa vegetation feedbacks to latitudinal temperature in (d) S125K_NA$_{VEC}$ and (e) S125K_NA$_{LPJ}$ compared to global vegetation feedbacks. In (d), the blue dot-line indicates 125 ka BP global vegetation feedbacks in LIG_VEC to latitudinal temperature; the blue and orange diamond-line indicates 125 ka BP North Africa vegetation feedbacks to latitudinal temperature in S125K_NA$_{VEC}$ and S125K_NA$_{GRASS}$, respectively; likewise, in (e), the green dot-line indicates 125 ka BP global vegetation feedbacks in LIG_LPJ to latitudinal temperature; the green and orange diamond-line indicates 125 ka BP North Africa vegetation feedbacks to latitudinal temperature in S125K_NA$_{LPJ}$ and S125K_NA$_{GRASS}$, respectively. (For interpretation of the references to color in this figure legend, the reader is referred to the Web version of this article.)

feedbacks in LPJ-GUESS would be somewhere in between the strongest and weakest values. In order to investigate the magnitude of vegetation feedbacks to climate during the LIG, we need to understand the range of vegetation responses and therefore call for more vegetation simulations with DGVMs of different complexities.

Another reason of the difference could be related to the asynchronous coupling of LPJ-GUESS to ECBilt. LPJ-GUESS simulates dynamical vegetation responding to climate changes, but in this asynchronous coupling process, the simulated vegetation is averaged every 10 years and passed back to ECBilt as static land surface parameters. Hence, the transition from green Sahara to desert is easily smoothed, and the feedback is thereby underestimated. Although our LIG simulations suggest consistent vegetation evolutions and positive vegetation feedbacks during the LIG with previous studies, we prefer the full dynamical coupling of LPJ-GUESS to ECBilt in the future to enhance the robustness in climate-vegetation interaction simulations. More simulations with vegetation in fully coupled climate models would help to narrow down the range of vegetation responses and feedbacks during the LIG.

4. Conclusions

In this study, we simulate the LIG climate and vegetation changes to investigate our three scientific questions using the climate model iLOVECLIM in which the vegetation component is either the fully coupled VECODE model or the asynchronously coupled LPJ-GUESS model. We address three scientific questions: 1) How abrupt is the 'green-to-desert' vegetation transition in the Sahara during the LIG? 2) To what extent are discrepancies between reconstructions and simulations related to vegetation feedbacks in the Sahara? 3) And what is the magnitude of dynamic vegetation feedbacks during the LIG? We conclude the following:

1) We simulate a relatively high vegetation cover (>70%) in the Sahara during the early LIG when the summer insolation at 20°N is relative high; followed by a desertification phase after 123 ka BP. The rates of desert expansion in the Sahara peak at 122 ka BP in both LIG_VEC (25%/ka) and LIG_LPJ (15%/ka), responding to the fast decline in 20°N July insolation, but the desertification in LIG_VEC (from 123 ka BP to 121 ka BP) is faster than in LIG_LPJ (from 123 ka BP to about 119 ka BP). This AHP termination is

accelerated when the magnitude of positive vegetation feedbacks on precipitation cannot offset the moisture deficit due to decreased summer insolation.

2) The simulated early LIG (125 ka BP) with fixed preindustrial vegetation (LIG_FIX) is consistent in its main features with multi-model simulations performed by others, and underestimates the proxy-based temperatures. Dynamically including LIG vegetation in simulations provides much better agreement with the temperature proxies than LIG_FIX, in particular in the high latitudes and the tropics. In boreal regions, trees extend further north and tree covers are up to 50% higher in 125 ka BP relative to pre-industrial conditions, resulting in a positive surface temperature anomaly (>2.5 °C) compared to pre-industrial. Likewise, in North Africa, positive surface temperature anomalies (~1.5 °C) are found. The stronger annual mean temperature trend during the LIG in simulations with dynamical vegetation at all latitudes indicates a warming effect of vegetation at a global scale, but they still underestimate the change in temperature compared to reconstructions.
3) At a local scale, the magnitude of vegetation feedbacks to climate peak at the early LIG and decrease during the LIG, corresponding to the vegetation changes. At a global scale, the green Sahara feedback provides 30% of the total contribution of global vegetation feedbacks to high latitudinal warming.

At a local scale, during the early LIG, the amounts of North African precipitation in simulations (LIG_VEC and LIG_LPJ) with dynamical vegetation (~60 cm/yr) are about twice as large as in a simulation (LIG_FIX) with fixed pre-industrial vegetation (~30 cm/yr), and surface temperatures are higher by about 2.5 °C in LIG_VEC and LIG_LPJ (31.5 °C). From 123 ka BP, the effects of vegetation feedbacks to climate decrease, which are in phase as vegetation collapses in LIG_VEC and LIG_LPJ. In LIG_VEC, the feedback to precipitation declines by 21 cm/yr from 123 ka BP to 121 ka BP, with <1 cm/yr after 121 ka BP. In LIG_LPJ, this feedback also declines rapidly from 123 ka BP to 121 ka BP by 15 cm/yr, following a slower decline from 8 cm/yr to <1 cm/yr from 121 ka BP to 119 ka BP. Likewise, the vegetation feedback to temperature keeps reducing from 2.8 °C to 2.0 °C in LIG_LPJ, while it reduces from 2.5 °C to 0 °C and becomes slightly negative after 121ka BP in LIG_VEC.

Author statement

Huan Li, Hans Renssen and Didier M. Roche: Conceptualization, Methodology, Software, Formal analysis, Data Curation, Writing-original draft, Writing-review &editing, Visualization. All authors contributed substantially to this work.

Declaration of competing interest

The authors declare that they have no known competing financial interests or personal relationships that could have appeared to influence the work reported in this paper.

Acknowledgements

We sincerely appreciate the valuable comments and suggestions provided by the two anonymous reviewers and the editor which helped improve an earlier version of the manuscript. This work was supported by the China Scholarship Council. Didier M. Roche is supported by CNRS/INSV and by the Vrije Universiteit Amsterdam.

References

Andersen, K., Azuma, N., Barnola, J.M., Bigler, M., Biscaye, P., Caillon, N., Chappellaz, J., Clausen, H.B., Dahl-Jensen, D., Fischer, H., Flückiger, J., Fritzsche, D., Fujii, Y., Goto-Azuma, K., Grønvold, K., Gundestrup, N.S., Hansson, M., Huber, C., Hvidberg, C.S., Johnsen, S.J., Jonsell, U., Jouzel, J., Kipfstuhl, S., Landais, A., Leuenberger, M., Lorrain, R., Masson-Delmotte, V., Miller, H., Motoyama, H., Narita, H., Popp, T., Rasmussen, S.O., Raynaud, D., Rothlisberger, R., Ruth, U., Samyn, D., Schwander, J., Shoji, H., Siggard-Andersen, M.L., Steffensen, J.P., Stocker, T., Sveinbjornsdottir, A.E., Svensson, A., Takata, M., Tison, J.L., Thorsteinsson, T., Watanabe, O., Wilhelms, F., White, J.W.C., 2004. High-resolution record of Northern Hemisphere climate extending into the last interglacial period. Nature 431 (7005), 147–151.

Bakker, P., Masson-Delmotte, V., Martrat, B., Charbit, S., Renssen, H., Gröger, M., Krebs-Kanzow, U., Lohmann, G., Lunt, D.J., Pfeiffer, M., Phipps, S.J., Prange, M., Ritz, S.P., Schulz, M., Stenni, B., Stone, E.J., Varma, V., 2014. Temperature trends during the Present and Last Interglacial periods – a multi-model-data comparison. Quat. Sci. Rev. 99, 224–243.

Bakker, P., Renssen, H., 2014. Last interglacial model-data mismatch of thermal maximum temperatures partially explained. Clim. Past 10 (4), 1633–1644.

Bakker, P., Stone, E.J., Charbit, S., Gröger, M., Krebs-Kanzow, U., Ritz, S.P., Varma, V., Khon, V., Lunt, D.J., Mikolajewicz, U., Prange, M., Renssen, H., Schneider, B., Schulz, M., 2013. Last interglacial temperature evolution: a model inter-comparison. Clim. Past 9 (2), 605–619.

Bereiter, B., Eggleston, S., Schmitt, J., Nehrbass-Ahles, C., Stocker, T.F., Fischer, H., Kipfstuhl, S., Chappellaz, J., 2015. Revision of the EPICA Dome C CO2record from 800 to 600 kyr before present. Geophys. Res. Lett. 42 (2), 542–549.

Berger, A., 1978. Long-term variations of caloric insolation resulting from the earth's orbital elements. Quat. Res. 9, 139–167.

Braconnot, P., Harrison, S.P., Kageyama, M., Bartlein, P.J., Masson-Delmotte, V., Abe-Ouchi, A., Otto-Bliesner, B., Zhao, Y., 2012. Evaluation of climate models using palaeoclimatic data. Nat. Clim. Change 2 (6), 417–424.

Braconnot, P., Joussaume, S., Marti, O., de Noblet, N., 1999. Synergistic feedbacks from ocean and vegetation on the African Monsoon response to Mid-Holocene insolation. Geophys. Res. Lett. 26 (16), 2481–2484.

Brovkin, V., Ganopolski, A., Svirezhev, Y., 1997. A continuous climate-vegetation classification for use in climate-biosphere studies. Ecol. Model. 101, 251–261.

Calov, R., Ganopolski, A., Petoukhov, V., Claussen, M., Brovkin, V., Kubatzki, C., 2005. Transient simulation of the last glacial inception. Part II: sensitivity and feedback analysis. Clim. Dynam. 24 (6), 563–576.

CAPE-members, Anderson, P., Bennike, O., Bigelow, N., Brigham-Grette, J., Duvall, M., Edwards, M., Fr'echette, B., Funder, S., Johnsen, S., Knies, J., Koerner, R., Lozhkin, A., MacDonald, G., Marshall, S., Matthiessen, J., Miller, G., Montoya, M., Muhs, D., Otto-Bliesner, B., Overpeck, J., Reeh, N., Sejrup, H.P., Turner, C., Velichko, A., 2006. Last Interglacial Arctic warmth confirms polar amplification of climate change. Quat. Sci. Rev. 25, 1383–1400. https://doi.org/10.1016/j.quascirev.2006.01.033.

Charney, J.G., 1975. Dynamics of deserts and drought in Sahel. Quarterly Journal ofthe Royal Meteorological Society 101 (428), 193–202.

Claussen, M., 1994. Coupling global biome models with climate models. Clim. Res. 4, 203–221.

Claussen, M., 1997. Modeling bio-geophysical feedback in the African and Indian-monsoon region. Clim. Dynam. 13 (4), 247–257.

Claussen, M., 2009. Late Quaternary vegetation-climate feedbacks. Clim. Past 5 (2), 203–216.

Claussen, M., Kubatzki, C., Brovkin, V., Ganopolski, A., Hoelzmann, P., Pachur, H.-J., 1999. Simulation of an abrupt change in Saharan vegetation in the Mid-Holocene. Geophys. Res. Lett. 26 (14), 2037–2040.

Claussen, M., Bathiany, S., Brovkin, V., Kleinen, T., 2013. Simulated climate-vegetation interaction in semi-arid regions affected by plant diversity. Nat. Geosci. 6 (11), 954–958.

Claussen, M., Gayler, V., 1997. The greening of the Sahara during the mid-Holocene: results of an interactive atmosphere-biome model. Global Ecol. Biogeogr. Lett. 6, 369–377.

Crucifix, M., Loutre, F., 2002. Transient simulations over the last interglacial period (126-115 kyr BP): feedback and forcing analysis. Clim. Dynam. 19 (5–6), 417–433.

Davies, F.J., Renssen, H., Blaschek, M., Muschitiello, F., 2015. The impact of Sahara desertification on Arctic cooling during the Holocene. Clim. Past 11 (3), 571–586.

Eltahir, E.A.B., 1996. Role of vegetation in sustaining large-scale atmospheric circulations in the tropics. J. Geophys. Res.: Atmosphere 101 (D2), 4255–4268.

Eltahir, E.A.B., Gong, C., 1996. Dynamics of wet and dry years in West Africa. J. Clim. 9 (5), 1030–1042.

Fischer, N., Jungclaus, J.H., 2010. Effects of orbital forcing on atmosphere and ocean heat transports in Holocene and Eemian climate simulations with a comprehensive Earth system model. Clim. Past 6, 155–168.

Fleitmann, D., Burns, S.J., Pekala, M., Mangini, A., Al-Subbary, A., Al-Aowah, M., Kramers, J., Matter, A., 2011. Holocene and Pleistocene pluvial periods in Yemen, southern Arabia. Quat. Sci. Rev. 30 (7–8), 783–787.

Goosse, H., Brovkin, V., Fichefet, T., Haarsma, R., Huybrechts, P., Jongma, J., Mouchet, A., Selten, F., Barriat, P.Y., Campin, J.M., Deleersnijder, E., Driesschaert, E., Goelzer, H., Janssens, I., Loutre, M.F., Morales Maqueda, M.A., Opsteegh, T., Mathieu, P.P., Munhoven, G., Pettersson, E.J., Renssen, H., Roche, D.M., Schaeffer, M., Tartinville, B., Timmermann, A., Weber, S.L., 2010. Description of the Earth system model of intermediate complexity LOVECLIM version 1.2. Geosci. Model Dev. (GMD) 3 (2), 603–633.

Govin, A., Braconnot, P., Capron, E., Cortijo, E., Duplessy, J.C., Jansen, E., Labeyrie, L.,

Landais, A., Marti, O., Michel, E., Mosquet, E., Risebrobakken, B., Swingedouw, D., Waelbroeck, C., 2012. Persistent influence of ice sheet melting on high northern latitude climate during the early Last Interglacial. Clim. Past 8 (2), 483–507.
Gröger, M., Maier-Reimer, E., Mikolajewicz, U., Schurgers, G., Vizcaíno, M., Winguth, A., 2007. Vegetation-climate feedbacks in transient simulations over the last interglacial (128000-113000 yrBP). Dev. Quat. Sci. (7), 563–572.
Haxeltine, A., Prentice, I.C., 1996. BIOME3: an equilibrium terrestrial biosphere model based on ecophysiological constraints, resource availability, and competition among plant functional types. Global Biogeochem. Cycles 10 (4), 693–709.
Hély, C., Lézine, A.M., contributors, A.P.D., 2014. Holocene changes in African vegetation: tradeoff between climate and water availability. Clim. Past 10 (2), 681–686.
Hoelzmann, P., Jolly, D., Harrison, S.P., Laarif, F., Bonnefille, R., Pachur, H.J., 1998. Mid-Holocene land-surface conditions in northern Africa and the Arabian Peninsula: a data set for the analysis of biogeophysical feedbacks in the climate system. Global Biogeochem. Cycles 12 (1), 35–51.
IPCC, 2013. Contribution of Working Groups I, II and III to the Fifth Assessment Report of the Intergovernmental Panel on Climate Change. Cambridge University Press, Geneva, Switzerland. Climate Change 2013: Synthesis Report. IPCC.
Jolly, D., Prentice, I.C., Bonnefille, R., Ballouche, A., Bengo, M., Brenac, P., Buchet, G., Burney, D., Cazet, J.P., Cheddadi, R., Edorh, T., Elenga, H., Elmoutaki, S., Guiot, J., Laarif, F., Lamb, H., Lezine, A.M., Maley, J., Mbenza, M., Peyron, O., Reille, M., Reynaud-Farrera, I., Riollet, G., Ritchie, J.C., Roche, E., Scott, L., Semmanda, I., Straka, H., Umer, M., Van Campo, E., Vilimumbalo, S., Vincens, A., Waller, M., 1998. Biome reconstruction from pollen and plant macrofossil data for Africa and the Arabian peninsula at 0 and 6000 years. J. Biogeogr. 25, 1007–1027.
Kopp, R.E., Simons, F.J., Mitrovica, J.X., Maloof, A.C., Oppenheimer, M., 2009. Probabilistic assessment of sea level during the last interglacial stage. Nature 462 (7275), 863–867.
Kutzbach, J.E., Guan, J., He, F., Cohen, A.S., Orland, I.J., Chen, G.S., 2020. African climate response to orbital and glacial forcing in 140,000-y simulation with implications for early modern human environments. Proc. Natl. Acad. Sci. Unit. States Am. 117 (5), 2255–2264.
Langebroek, P.M., Nisancioglu, K.H., 2014. Simulating last interglacial climate with NorESM: role of insolation and greenhouse gases in the timing of peak warmth. Clim. Past 10 (4), 1305–1318.
Larrasoana, J.C., Roberts, A.P., Rohling, E.J., 2013. Dynamics of green Sahara periods and their role in hominin evolution. PloS One 8 (10), e76514. https://doi.org/10.1371/journal.pone.0076514.
Lézine, A.-M., Hély, C., Grenier, C., Braconnot, P., Krinner, G., 2011. Sahara and Sahel vulnerability to climate changes, lessons from Holocene hydrological data. Quat. Sci. Rev. 30 (21–22), 3001–3012.
Li, H.H., Renssen, D.M., Roche, 2019. Global vegetation distribution driving factors in two DynamicGlobal Vegetation Models of contrasting complexities. Global Planet. Change. https://doi.org/10.1016/j.gloplacha.2019.05.009.
Liu, Z., Wang, Y., Gallimore, R., Notaro, M., Prentice, I.C., 2006. On the cause of abrupt vegetation collapse in North Africa during the Holocene: climate variability vs. vegetation feedback. Geophys. Res. Lett. 33 (22).
Loulergue, L., Schilt, A., Spahni, R., Masson-Delmotte, V., Blunier, T., Lemieux, B., Barnola, J.M., Raynaud, D., Stocker, T.F., Chappellaz, J., 2008. Orbital and millennial-scale features of atmospheric CH_4 over the past 800,000 years. Nature 453 (7193), 383–386.
LUH2, 2012. World Climate Research Program Coupled Intercomparison Project (CMIP6). Land-Use Harmonisation 2. Dataset at. http://luh.emd.edu/data.shtml.
Lunt, D.J., Abe-Ouchi, A., Bakker, P., Berger, A., Braconnot, P., Charbit, S., Fischer, N., Herold, N., Jungclaus, J.H., Khon, V.C., Krebs-Kanzow, U., Langebroek, P.M., Lohmann, G., Nisancioglu, K.H., Otto-Bliesner, B.L., Park, W., Pfeiffer, M., Phipps, S.J., Prange, M., Rachmayani, R., Renssen, H., Rosenbloom, N., Schneider, B., Stone, E.J., Takahashi, K., Wei, W., Yin, Q., Zhang, Z.S., 2013. A multi-model assessment of last interglacial temperatures. Clim. Past 9 (2), 699–717.
Masson-Delmotte, V., Schulz, M., Abe-Ouchi, A., et al., 2013. Information from paleoclimate archives. In: Stocker, T.F., Qin, D., Plattner, G.-K., et al. (Eds.), Climate Change 2013: the Physical Science Basis. Contribution of Working Group I to the Fifth Assessment Report of the Intergovernmental Panel on Climate Change. Cambridge University Press, Cambridge, pp. 383–464.
McKay, N.P., Overpeck, J.T., Otto-Bliesner, B.L., 2011. The role of ocean thermal expansion in Last Interglacial sea level rise. Geophys. Res. Lett. 38 (14) https://doi.org/10.1029/2011GL048280.
Muschitiello, F., Zhang, Q., Sundqvist, H.S., Davies, F.J., Renssen, H., 2015. Arctic climate response to the termination of the african Humid Period. Quat. Sci. Rev. 125, 91–97.
Nikolova, I., Yin, Q., Berger, A., Singh, U.K., Karami, M.P., 2013. The last interglacial (Eemian) climate simulated by LOVECLIM and CCSM3. Clim. Past 9 (4), 1789–1806.
Notaro, M., Wang, Y.I., Liu, Z., Gallimore, R., Levis, S., 2008. Combined statistical and dynamical assessment of simulated vegetation-rainfall interactions in North Africa during the mid-Holocene1. Global Change Biol. 14 (2), 347–368.
Opsteegh, J.D., Haarsma, R.J., Selten, F.M., Kattenberg, A., 1998. ECBILT: a dynamic alternative to mixed boundary conditions in ocean models. Tellus 50 (3), 348–367.
Osborne, A.H., Vance, D., Rohling, E.J., Barton, N., Rogerson, M., Fello, N., 2008. A humid corridor across the Sahara for the migration of early modern humans out of Africa 120,000 years ago. Proc Natl AcadSci U S A 105 (43), 16444–16447.
Otto-Bliesner, B.L., Braconnot, P., Harrison, S.P., Lunt, D.J., Abe-Ouchi, A., Albani, S., Bartlein, P.J., Capron, E., Carlson, A.E., Dutton, A., Fischer, H., Goelzer, H., Govin, A., Haywood, A., Joos, F., LeGrande, A.N., Lipscomb, W.H., Lohmann, G., Mahowald, N., Nehrbass-Ahles, C., Pausata, F.S.R., Peterschmitt, J.-Y., Phipps, S.J., Renssen, H., Zhang, Q., 2017. The PMIP4 contribution to CMIP6 – Part 2: two interglacials, scientific objective and experimental design for Holocene and Last Interglacial simulations. Geosci. Model Dev. (GMD) 10 (11), 3979–4003.
Otto-Bliesner, B.L., Brady, E.C., Zhao, A., Brierley, C., Axford, Y., Capron, E., Govin, A., Hoffman, J., Isaacs, E., Kageyama, M., Scussolini, P., Tzedakis, P.C., Williams, C., Wolff, E., Abe-Ouchi, A., Braconnot, P., Ramos Buarque, S., Cao, J., de Vernal, A., Guarino, M.V., Guo, C., LeGrande, A.N., Lohmann, G., Meissner, K., Menviel, L., Nisancioglu, K., O'ishi, R., Salas, Y., Melia, D., Shi, X., Sicard, M., Sime, L., Tomas, R., Volodin, E., Yeung, N., Zhang, Q., Zhang, Z., Zheng, W., 2019. Large-scale features of Last Interglacial climate: Results from evaluating the lig127k simulations for CMIP6-PMIP4. Clim. Past Discuss. https://doi.org/10.5194/cp-2019-174.
Otto-Bliesner, B.L., Rosenbloom, N., Stone, E.J., McKay, N.P., Lunt, D.J., Brady, E.C., Overpeck, J.T., 2013. How warm was the last interglacial? New model-data comparisons. Philos Trans A Math Phys EngSci 371 (2001), 20130097.
Pedersen, R.A., Langen, P.L., Vinther, B.M., 2017. The last interglacial climate: comparing direct and indirect impacts of insolation changes. Clim. Dynam. 48 (9–10), 3391–3407.
Petoukhov, V., Ganopolski, A., Brovkin, V., Claussen, M., Eliseev, A., Kubatzki, C., Rahmstorf, S., 2000. CLIMBER-2: a climate system model of intermediate complexity. Part I: model description and performance for present climate. Clim. Dynam. 16, 1–17.
PMIP4, 2017. Paleoclimate modeling Intercomparison Project4 forcing dataset at. https://pmip4.lsce.ipsl.fr/doku.php/data:index.
Prentice, I.C., Jolly, D., 2000. Mid-Holocene and glacial-maximum vegetation geography of the northern continents and Africa. Biome 6000 participants, J. Biogeogr. 27, 507–519.
Renssen, H., Brovkin, V., Fichefet, T., Goosse, H., 2003. Holocene climate instability during the termination of the african Humid Period. Geophys. Res. Lett. 30 (4) https://doi.org/10.1029/2002GL016636.
Renssen, H., Brovkin, V., Fichefet, T., Goosse, H., 2006. Simulation of the Holocene climate evolution in northern Africa: the termination of the african Humid Period. Quat. Int. 150 (1), 95–102.
Roche, D.M., Dumas, C., Bügelmayer, M., Charbit, S., Ritz, C., 2014. Adding a dynamical cryosphere to iLOVECLIM (version 1.0): coupling with the GRISLI ice-sheet model. Geosci. Model Dev. (GMD) 7 (4), 1377–1394.
Rohling, E.J., Cane, R., Cooke, S., Sprovieri, M., Bouloubassi, I., Emeis, K.C., Schiebel, R., Kroon, D., Jorissen, F.J., Lorre, A., Kemp, A.E.S., 2002. African monsoon variability during the previous interglacial maximum. Earth Planet Sci. Lett. 202, 61–75.
Sanchez Goni, M.F., Bakker, P., Desprat, S., Carlson, A.E., Van Meerbeeck, C.J., Peyron, O., Naughton, F., Fletcher, W.J., Eynaud, F., Rossignol, L., Renssen, H., 2012. European climate optimum and enhanced Greenland melt during the Last Interglacial. Geology 40 (7), 627–630.
Saraswat, R., Lea, D.W., Nigam, R., Mackensen, A., Naik, D.K., 2013. Deglaciation in the tropical Indian Ocean driven by interplay between the regional monsoon and global teleconnections. Earth Planet Sci. Lett. 375, 166–175.
Schilt, A., Baumgartner, M., Blunier, T., Schwander, J., Spahni, R., Fischer, H., Stocker, T.F., 2010a. Glacial–interglacial and millennial-scale variations in the atmospheric nitrous oxide concentration during the last 800,000 years. Quat. Sci. Rev. 29 (1–2), 182–192.
Schilt, A., Baumgartner, M., Schwander, J., Buiron, D., Capron, E., Chappellaz, J., Loulergue, L., Schüpbach, S., Spahni, R., Fischer, H., Stocker, T.F., 2010b. Atmospheric nitrous oxide during the last 140,000years. Earth Planet Sci. Lett. 300 (1–2), 33–43.
Schneider, R., Schmitt, J., Köhler, P., Joos, F., Fischer, H., 2013. A reconstruction of atmospheric carbon dioxide and its stable carbon isotopic composition from the penultimate glacial maximum to the last glacial inception. Clim. Past 9, 2507–2523. https://doi.org/10.5194/cp-9-2507-2013.
Schurgers, G., Mikolajewicz, U., Groger, M., Maier-Reimer, E., Vizcaıno, M., Winguth, A., 2006. Dynamics of the terrestrial biosphere, climate and atmospheric CO2 concentration during interglacials: a comparison between Eemian and Holocene. Clim. Past 2, 205–220. https://doi.org/10.5194/cp-2-205-2006.
Schurgers, G., Mikolajewicz, U., Gröger, M., Maier-Reimer, E., Vizcaíno, M., Winguth, A., 2007. The effect of land surface changes on Eemian climate. Clim. Dynam. 29 (4), 357–373.
Smith, B., Prentice, I.C., Sykes, M.T., 2001. Representation of vegetation dynamics in the modelling of terrestrial ecosystems: comparing two contrasting approaches within European climate space. Global Ecol. Biogeogr. 10 (6), 621–637.
Smith, B., Wårlind, D., Arneth, A., Hickler, T., Leadley, P., Siltberg, J., Zaehle, S., 2014. Implications of incorporating N cycling and N limitations on primary production in an individual-based dynamic vegetation model. Biogeosciences 11, 2027–2054.
Tierney, J.E., Pausata, F.S.R., deMenocal, P.B., 2017. Rainfall regimes of the green Sahara. Sci. Adv. 3 (1), e1601503.
Timm, O., Köhler, P., Timmermann, A., Menviel, L., 2010. Mechanisms for the onset of the african Humid Period and Sahara greening 14.5–11 ka BP. J. Clim. 23 (10), 2612–2633.
Turney, C.S.M., Jones, R.T., 2010. Does the Agulhas Current amplify global temperatures during super-interglacials? J. Quat. Sci. 25 (6), 839–843.